

Computational Studies of Horizontal Axis Wind Turbines

Annual Status Report

Covering the period

May 6, 1999 – May 5, 2000

Contract No. XCX-7-16466-02

Submitted to the

National Renewable Energy Laboratory
Attn: Dr. Scott Schreck
1617 Cole Boulevard
Golden, CO 80401-3393

Prepared by

Lakshmi N. Sankar
School of Aerospace Engineering
Georgia Institute of Technology
Atlanta, GA 30332-0150

May 4, 2001

I. INTRODUCTION

A computational research program is underway at Georgia Tech in the area of horizontal-axis wind turbine aerodynamics. The research focuses on understanding the flow mechanisms that affect the performance of wind turbines in non-axial and non-uniform inflow, and the development of modern, efficient computational techniques that complement existing combined blade element-momentum theory.

The computational effort is based on the extension of a 3-D hybrid Navier-Stokes/potential flow solver that has been developed at Georgia Tech for helicopter rotor and propeller applications to horizontal axis wind turbines. In this approach three-dimensional unsteady compressible Navier-Stokes equations are solved in a small region, on a body-fitted grid surrounding the rotor blade. Away from the blades, the potential flow equation is solved. The vorticity shed by the blades as a result of dynamic stall, and the spanwise and azimuthal variations of circulation are captured using vortex filaments. These filaments are freely convected by the local flow. Since the costly Navier-Stokes calculations are done only in regions close to the wind turbine blades, and because much of the vorticity is tracked using Lagrangean techniques, this method is an order of magnitude more efficient than full blown Navier-Stokes methods.

SUMMARY OF ACTIVITIES DURING THE RESEARCH PERIOD

During this reporting period (May 6, 1999 - May 5, 2000), work was done in the following areas.

1. Two turbulence models (Spalart-Allmaras, Baldwin-Lomax) and two transition models (Eppler's, Michel's) were developed and applied to NREL Phase II and Phase III rotors.
2. The effects of yaw (non-axial wind) on the rotor performance were studied.
3. A version of the present analysis capable of modeling tower shadow effects was developed, and validated.

These studies have been documented in detail in the quarterly progress reports submitted to NREL. Some of these results were also presented as a paper at the AIAA/ASME Wind Energy Symposium in Reno, on January 2000 (AIAA 2000-0048). A copy of this paper is included here.

Effects of Transition, Turbulence and Yaw on the Performance of Horizontal Axis Wind Turbines

Guanpeng Xu¹ and Lakshmi N. Sankar²
School of Aerospace Engineering
Georgia Institute of Technology, Atlanta, GA 30332-0150

ABSTRACT

Recent improvements to the capabilities of a hybrid Navier-Stokes potential flow methodology for modeling horizontal axis wind turbine (HAWT) configurations are presented. The study focuses on three issues: the effects of turbulence models and transition models, the effects of prescribed wake states on predicted rotor performance, and the effects of non-axial flow (yaw) on power generation. Comparisons with measured data for a rotor tested at the National Renewable Energy Laboratory (NREL) is presented.

INTRODUCTION

A computational research effort is underway at Georgia Tech in the area of horizontal-axis wind-turbine aerodynamics. The research focuses on understanding the flow mechanisms that affect the performance of wind turbines in non-axial and non-uniform inflow. The effort also addresses the development of efficient computational techniques that complement existing combined blade element-momentum theory methods.

This work is an extension of a 3-D hybrid Navier-Stokes/potential flow solver that has been developed at Georgia Tech for horizontal axis wind turbines (HAWT). In this approach the three-dimensional unsteady compressible Navier-Stokes equations are solved only in a small region, on a body-fitted grid surrounding the rotor blade. Away from the blades, the potential flow equation is solved. The vorticity shed from the blades is modeled as vortex filaments once the vorticity leaves the Navier-Stokes region. These filaments are freely convected by the local flow. Since the costly Navier-Stokes calculations are done only in regions close to the wind turbine blades, and because much of the vorticity is tracked using Lagrangean techniques, this method is an order of magnitude more efficient than Navier-Stokes methods.

The basic hybrid Navier-Stokes potential flow methodology and its application to HAWT under axial-flow conditions are documented in AIAA-99-0042 (Xu and Sankar, 1999).

SCOPE OF THE PRESENT STUDY

This paper describes recent enhancements to the flow solver, and applications to configurations of interest. The enhancements focused on the following three areas: transition and turbulence modeling, physically consistent wake modeling, and modeling of yaw effects. These three areas are briefly discussed below.

Transition and Turbulence Modeling Issues:

Studies were done to assess the effects of two turbulence models and two transition models on the predicted performance. A one-equation Spalart-Allmaras turbulence model (Shur et al. 1998) and the baseline zero-equation Baldwin-Lomax turbulence model were studied.

As a consequence of the low relative velocities and small chord lengths encountered in HAWT systems, a significant portion of the boundary layer over the blade can be laminar. The location of the transition line affects the profile power consumed by the rotor, and can impact the power generation. To predict the transition position, two existing transition models, one by Eppler, and a second based on Michel's criterion, were used. The Eppler model is used in many NREL sponsored design codes, and is an obvious first candidate for transition prediction. Michel's criterion (Michel 1984) is developed based on measurements in two-dimensional, incompressible flow. These models are used in many aircraft industry boundary layer codes, such as those developed by Tuncer Cebeci (1989).

¹ Ph.D. candidate, AIAA member

² Regents' professor, Associate Fellow AIAA

Wake Geometry Modeling:

The prescribed wake model in the hybrid Navier-Stokes/Potential flow analysis has been modified to properly reflect the states that a rotor can assume, as the wind speed changes. It is based on the theory and phenomenology of rotor states, which was presented by Glauert (1937) and was extended by Wilson and Lissaman (1972) to wind rotors.

Yaw Effects:

Finally, a numerical procedure for modeling skewed wind (yaw) conditions has been developed. As in axial flow simulations, the yaw calculations only need to model the aerodynamics of a single blade. Other blades will experience the same load and flow pattern 1/N revolutions later, where N is the number of blades. For a three-bladed rotor the computational domain covers a 120° portion of the rotor disk. The present procedure thus retains the efficiency of hybrid method even for yaw conditions. In contrast to the hybrid method, a full Navier-Stokes solver would require the modeling of all blades, significantly increasing the computational effort.

MATHEMATICAL AND NUMERICAL FORMULATION

A complete description of the hybrid theory behind the present hybrid approach is given in AIAA-99-0042 (Xu and Sankar, 1999). Sankar and his coworkers have also used the hybrid procedure in several fixed and rotary wing solvers. For this reason, only the turbulence and transition model enhancements, and the extension of the flow solver to yaw conditions are presented here.

Spalart-Allmaras Turbulence Model:

The first enhancement to the hybrid analysis was the replacement of a simple algebraic eddy viscosity model with a phenomenological one-equation eddy viscosity model called the Spalart-Allmaras model.

In this model, the Reynolds stresses are given by

$$-\overline{u_i u_j} = 2\nu_t S_{ij} \quad (1)$$

Where

$$S_{ij} \equiv (\partial U_i / \partial x_j + \partial U_j / \partial x_i) / 2 \quad (2)$$

The eddy viscosity ν_t is given by

$$\nu_t = \tilde{\nu} f_{v1} \quad (3)$$

Where,

$$f_{v1} = \frac{\chi^3}{\chi^3 + c_{v1}^3} \quad \text{And, } \mathbf{c} \equiv \frac{\tilde{\mathbf{n}}}{\mathbf{n}}$$

Here \mathbf{v} is the molecular viscosity. The quantity $\tilde{\mathbf{n}}$ is the working variable and obeys the transport equation.

$$\frac{D\tilde{\mathbf{n}}}{Dt} = c_{b1} [1 - f_{t2}] \tilde{S} \tilde{\mathbf{n}} + \frac{1}{S} [\nabla \cdot ((\mathbf{n} + \tilde{\mathbf{n}}) \nabla \tilde{\mathbf{n}}) + c_{b2} (\nabla \tilde{\mathbf{n}})^2] - \left[c_w f_w - \frac{c_{b1}}{\kappa^2} f_{t2} \right] \left[\frac{\tilde{\mathbf{n}}}{d} \right] + f_{t1} \Delta U^2 \quad (4)$$

Here S is the magnitude of the vorticity, and

$$\tilde{S} \equiv S + \frac{\tilde{\mathbf{v}}}{\kappa^2 d^2} f_{v2} \quad (5)$$

Also, d is the distance to the closest wall, and,

$$f_{v2} = 1 - \frac{\chi}{1 + \chi f_{v1}} \quad (6)$$

The function f_w is given by the following expression:

$$f_w = g \left[\frac{1 + c_{w3}^6}{g^6 + c_{w3}^6} \right]^{1/6} \quad (7)$$

Where

$$g = r + c_{w2} (r^6 - r) \quad (8)$$

And

$$r \equiv \frac{\tilde{\mathbf{v}}}{\tilde{S} \kappa^2 d^2} \quad (9)$$

For large values of r, f_w asymptotically reaches a constant value; therefore, large values of r can be truncated to 10 or so.

The Wall boundary condition is $\tilde{\mathbf{v}} = 0$. In the freestream $\tilde{\mathbf{v}} = 0$ is found to work best, provided numerical errors do not push $\tilde{\mathbf{v}}$ to negative values near the edge of the boundary layer. Values below $\nu/10$ are acceptable.

The Spalart-Allmaras model has a built-in provision for driving the eddy viscosity to zero upstream of the transition point. This is done by the f_{t2} function, which goes to unity upstream of the transition point.

$$f_{t2} = c_{t3} \exp(-c_{t4} \chi^2) \quad (10)$$

The trip function f_{t1} is computed as follows. Let d_t be the distance from the field point to the trip location, which is on a wall. Let the quantity ω_t be the wall vorticity at the trip location, and ΔU the difference between the velocity at the field point and that at the trip. Then one can compute an intermediate quantity $g_t = \min(0.1, \Delta U / \omega_t \Delta x)$ where Δx is the grid spacing along the wall at the trip location. Finally,

$$f_{t1} = c_{t1} g_t \exp\left(-c_{t2} \frac{\omega_t^2}{\Delta U^2} [d^2 + g_t^2 d_t^2]\right) \quad (11)$$

The constants are:

$$c_{b1}=0.1355, \sigma=2/3, c_{b2}=0.622, \kappa=0.41, \\ c_{\omega1} = c_{b1}/\kappa^2 + (1 + c_{b2})/\sigma, c_{\omega2}=0.3, c_{\omega3}=2, \\ c_{v1}=7.1, c_{t1} = 1, c_{t2} = 2, c_{t3} = 1.1, c_{t4} = 2.$$

Further details on the Spalart-Allmaras model are given by Shur et al. (1998).

Eppler Transition Prediction Model

The second enhancement to the hybrid method was the incorporation of transition line prediction models. Two models, one by Eppler, and the second by Michel have been investigated.

The Eppler's transition model was implemented in the hybrid Navier-Stokes/Potential flow analysis, in the following manner. Every 10 time steps or so, the surface pressure distribution on the turbine blade is passed to an integral boundary layer analysis, one radial location at a time. Inside the boundary layer analysis, the streamwise growth of laminar boundary layer quantities such as the momentum thickness θ , shape factor H , energy thickness δ_3 , and the factor $H_{32} = \delta_3/\theta$ are computed using Thwaites' method (Thwaites, 1949). Transition is predicted to occur if the Reynolds number based on the momentum thickness becomes large so that:

$$\log\left(\frac{u_e q}{n}\right) > 18.4H_{32} - 21.74 - 0.34r \quad (12)$$

Here u_e is the velocity at the edge of boundary layer, and 'r' is a roughness factor. For highly polished surfaces, r may be taken to be zero.

This model also predicts that transition has occurred if the laminar boundary layer separates, and forms a separation bubble near the leading edge of the rotor.

Chen-Thyson Transition Model and Michel's Criterion:

In this model, transition is said to occur at the chordwise location where the local Reynolds number based on the momentum thickness R_θ is related to the Reynolds number based on length R_x by,

$$R_\theta = 1.174 \left(1 + \frac{22400}{R_x}\right) R_x^{0.46} \quad (13)$$

In order to avoid an abrupt transition, Chen and Thyson recommend that the eddy viscosity be multiplied by the factor:

$$\gamma_{tr} = 1 - \exp\left[-G(x - x_{tr}) \int_{x_{tr}}^x \frac{dx}{u_e}\right] \quad (14)$$

Upstream of onset point of transition region, γ_{tr} is set to zero. The quantity G is computed from:

$$G = \left(\frac{3}{C^2}\right) \frac{u_e^3}{v^2} R_{x_{tr}}^{-1.34} \quad (15)$$

The transition Reynolds number is defined as:

$$R_{x_{tr}} = \left(\frac{u_e x}{v}\right)_{tr} \quad (16)$$

And,

$$C^2 = 213(\log R_{x_{tr}} - 4.7323) \quad (17)$$

It should be noted that the quantity R_x is based on the local freestream velocity (the magnitude of the vector sum of wind speed, induced velocity, and the blade velocity due to rotation $\vec{\Omega} \times \vec{r}$). Thus, for wind turbines,

$$R_x = \frac{u_{\infty local} x}{n} = \frac{c}{n} \frac{V_{tip}}{c} c V_{tip} = \left(\frac{x}{c}\right) \tilde{u}_{local} Re_{tip} \quad (18)$$

The non-dimensional velocity \tilde{u}_{local} is computed as,

$$\tilde{u}_{local} = \sqrt{\left(\frac{v_{wind} - v_i}{V_{tip}}\right)^2 + \left(\frac{r}{R}\right)^2} \quad (19)$$

Where r is the local radial distance from the hub, R is the tip radius, and x/c is non-dimensional x coordinate. Induced velocity v_i is estimated to a first order from the momentum theory. The Reynolds number based on the momentum thickness is also computed using the free-stream velocity, not the boundary layer edge velocity.

Methodology for Yaw Simulation

A numerical procedure for modeling off axis wind (yaw) conditions has been developed. As in axial flow calculations, the yaw calculations only need to model the aerodynamics of a single blade. Other blades will experience the same load and flow pattern 1/N revolutions later, where N is the number of blades. For a three-bladed rotor the computational domain covers a 120° portion of the rotor disk at a specific running time. The present procedure thus retains the efficiency of the hybrid method even for yaw conditions. In contrast to the hybrid method, a full Navier-Stokes solver would require the modeling of all blades, greatly increasing the computational effort.

When developing the first-principles based analysis for modeling rotors in cross flow, there are three kinds of non-axial flow (yaw) effects that should be addressed. First is the difference in the flow between the advancing and retreating sides due to the "edge-wise" velocity component in the plane of rotor disk. As shown in figure 1, the turbine blade experiences a higher relative velocity on the advancing side than on

the retreating side. This fluctuation in velocity produces fluctuations in the blade loads, and the power generated.

The second effect that must be modeled is the skewness of tip vortex wake as shown in figure 2. This results in an azimuthally non-uniform induced flow field at the rotor plane. Furthermore, the vorticity strength in the wake will vary with time, as the loads on the blade vary with time. This is in contrast to axial flow, where the blade loading is independent of the azimuthal location of the blade.

Finally, the analysis must include aeroelastic deformation of the rotor blades, and blade teetering and flapping motion, if any. Since the rotor tested by NREL uses stiff blades, the blade was assumed to be rigid without any cyclic pitching or flapping of the blades.

The present Hybrid methodology has been extended to simulation of yaw conditions. This method uses a skewed wake geometry to model yawed flow conditions. The skew angle is determined by the ratio between the inflow velocity (which is a combination of the induced velocity from momentum theory and the normal component of wind velocity), and the edgewise component of wind velocity.

A two step procedure has been used for modeling yaw effects. The first step simulates axial flow conditions at a given wind speed. When the hybrid code has converged, the tip vortex strength, and the wake geometry for the axial flow condition are saved. These quantities serve as the initial condition for the second step, where the wake geometry is skewed as discussed above, and the edgewise velocity component is applied to the "freestream" velocity.

At every 10 degree increments in azimuth, the peak bound circulation strength at that azimuthal angle is set to be the strength for all the tip vortex segments that were shed from all the blades when they were at that azimuthal angle. After two revolutions of the reference blade, the flow field may be considered to be well-developed and periodic.

Unlike the axial flow condition, the flow properties of the reference blade will not converge to a steady state solution in yaw. Repeatability of the blade loads from one revolution to the next is used as the criterion for convergence.

RESULTS AND DISCUSSION

Transition Model and Turbulence Model Studies:

The Eppler and Michel transition models, along with the Baldwin-Lomax and the Spalart-Allmaras turbulence models have been fully integrated into the Georgia Tech hybrid code. Figure 3 and Figure 4 show the prediction transition lines on the upper surface and lower surface for a wind turbine known as NREL Phase III rotor (Schepers 1997), operating at a wind speed of

6 m/s. The rotor operates at 72 rpm. At this low wind speed condition, the flow field behaves nicely, with attached flow over most of the rotor. In these figures, the legends '0 eqn' and '1 eqn' represent the Baldwin-Lomax and the Spalart-Allmaras models, respectively.

On both the upper and the lower surface, Eppler's model predicts a transition location that is upstream of Michel's predictions. Eppler's model, as implemented in the present code, first checks to see if laminar boundary layer has separated. If so, Eppler's model assumes that transition has occurred. Note that the inflexion point on the separated flow boundary layer will cause Tollmien-Schlichting instability to develop, causing transition. The Michel criterion, on the other hand, bases its transition criterion primarily on the boundary layer thickness. At this wind speed, the boundary layer has to grow up to 55% chord or so, before Michel's criterion detects transition.

On the lower surface, the pressure gradients tend to be more favorable than on the upper side. This leads to a thinner boundary layer and separation aft of the 40% chord. As a consequence, both these criteria predict that transition will occur aft of the corresponding upper surface locations.

The Reynolds number near the root is less than 10^5 . Both models predict that the flow will remain laminar all the way to the trailing edge near the root region. It is also observed that the transition line location is relatively insensitive to the turbulence model used.

Figure 5 shows the transition lines on the lower surface of the CER Phase III rotor at 8m/s. Even though the overall pattern of the transition lines is similar to the 6m/s case, the following differences may be observed:

- a) Michel's model predicts that the transition phenomenon over much of the lower surface is delayed, compared to the 6m/s case. This is attributable to the higher local angle of attack the blade sections operate in, and the favorable pressure gradients that exist on the windward side of the rotor.
- b) The Eppler transition model, on the other hand, predicts transition lines that are similar at the 8m/s and 6m/s conditions, presumably because laminar separation is detected in the vicinity of 40% chord at both these wind conditions. Notice that the maximum thickness location for the S-809 airfoil is near 40% chord. The pressure gradient tends to be favorable from the leading edge up to 40% chord, after which it becomes adverse at both these wind conditions.
- c) At the higher wind speed, a larger region near the root on the windward side remains laminar.
- d) The transition line predicted using the Michel's transition model in conjunction the Spalart-Allmaras turbulence model has a kink near the

33% radius. The reason for this behavior is not known at this writing.

Figure 6 shows the transition lines on the upper surface at 8m/s. Epppler's model predicts that transition will occur near the leading edge, as a result of leading edge separation. Michel's model, on the other hand, predicts transition around 50% chord, with a considerable radial variation in the transition location, especially near the root.

The large difference observed in the upper surface transition pattern of the rotor between the 8 m/s and the 6 m/s is attributable to the changes in the operating state of the turbine. For the Phase III rotor at 72 rpm, as the wind speed increase to around 8m/s, the operating state switches from a wind turbine state to a turbulent wake state (Wilson, R. E. et al., 1974).

Yaw Results

The hybrid code has been modified to account for three yaw effects as described earlier. The Phase III rotor was studied for a 10 m/s wind, and a 20-degree fixed yaw condition. Figure 7 shows the total power generated by all the three blades, taking into account the phase difference among the blades. The instantaneous power curve shows high frequency components superposed on a mean value. The power fluctuations are about 4% of the time-averaged power. The time-averaged values are in good agreement with NREL data.

Figure 7 is the result after Fourier filtering of the present results because the data from the simulation contain numerical noise. For example, in the present simulations, the wake induced velocity is updated once every 10 degrees of azimuth. This produces numerical noise at a wave number of 36, that must be filtered out.

Measurements for the Phase IV rotor of NREL were compared with results of Hybrid solver. The Phase IV rotor of NREL has the same geometry as the Phase III rotor, but has improved measurement devices. A time series of unsteady measurement lasts 16 seconds, or 18 revolutions of the rotor. The measured data not only includes the effects of yaw and unsteady wind inflow, but also other effects such as the tower shadow and wind shear. Figure 8 shows the unsteadiness of the measured wind.

Figure 9 compares the present hybrid method results with the measured data at five typical time intervals, each interval corresponding to one blade revolution. Both the computed data and the measurements show comparable fluctuations in the power, about comparable mean value.

CONCLUDING REMARKS

The Georgia Tech wind turbine code has been extensively modified. The transition from laminar flow

to turbulent flow is now modeled using empirical transition models. Phenomenological one-equation turbulence models have replaced algebraic turbulence models. The code has been modified to model yaw effects. Preliminary calculations done to validate these enhancements show that the predictions are consistent with measurements.

ACKNOWLEDGEMENTS

The National Renewable Energy Laboratory (NREL) supported this work. Alan Laxson and Scott Schreck of NREL, and Walter Wolfe of Sandia National Laboratory are the technical monitors.

REFERENCES

Tuncer Cebeci, "Essential Ingredients of a Method for Low Reynolds-Number Airfoils," AIAA Journal Vol. 27, No. 12, December 1989, pp. 1680-1685.

Chen, K. K., and Thyson, N. A., "Extension of Emmons' Spot Theory to Flow on Blunt Bodies," AIAA Journal, Vol. 9, 1971, pp. 821-825

Eggleston and Stoddard, Wind Turbine Engineering Design, ISBN 0-442-22195-9

Eppler, R., Airfoil Design and Data, New York, NY, Springer-Verlag, 1990, 562 pp.

Glauert, H. "Airplane Propellers," From Div. L, Aerodynamic Theory, ed. W. F. Durand, Berlin: Springer Verlag, 1935.

R. Michel, et al, "Stability Calculations and Transition Criteria on Two- or Three-Dimensional Flows," Laminar-Turbulent Transition, Novosibirsk, USSR, July 9-13, 1984, pp. 455-461.

Thwaites, B., "Approximate calculation of the laminar Boundary layer," Aeronautical Quarterly, Vol. 1, 1949, pp.245-280.

Schepers, et al "Final Report of IEA ANNEX XIV: Field Rotor Aerodynamics". Netherlands Energy Research Foundation, ECN-C-97-027

M. Shur, et al, "Turbulence Modeling in Rotating and Curved Channels: Assessment of the Spalart-Shur Correction Term," AIAA 98-0325.

Spalart, P. R., and Allmaras, S. R., "A One-Equation Turbulence Model for Aerodynamic Flows," AIAA-92-0439.

Wilson, R. E. and Lissaman, P. B. S., "Applied Aerodynamics of Wind Power Machines," Oregon State University, 1974.

Xu, G., and Sankar, L. N., "Computational Study of Horizontal Axis Wind Turbines," AIAA Paper 99-0042.

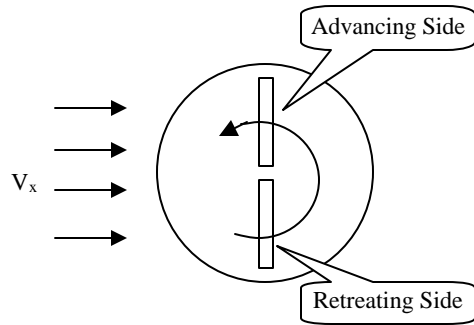


Figure 1: Relative Velocities in the Disk Plane

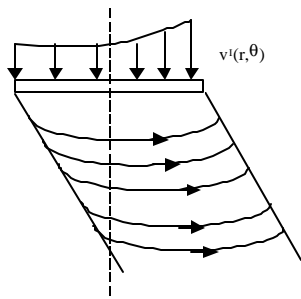


Figure 2. Schematic of the Skewed wake

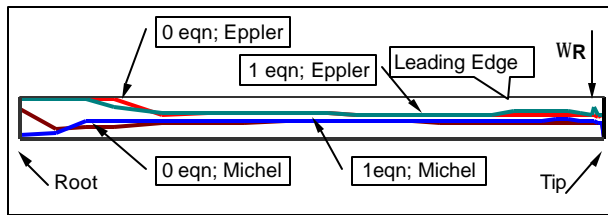


Fig. 3 Transition lines on upper surface of Phase III rotor in 6 m/s

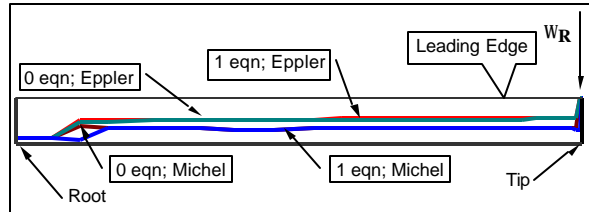


Fig. 4 Transition lines on lower surface of Phase III rotor in 6 m/s

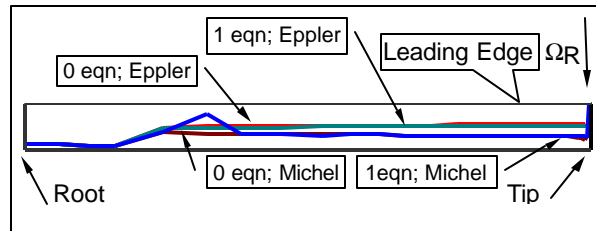


Fig. 5 Transition lines on lower surface of Phase III rotor in 8 m/s

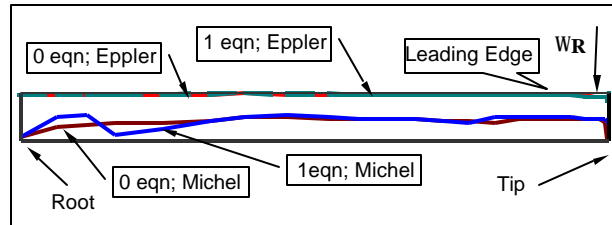


Fig. 6 Transition lines on upper surface of Phase III rotor in 8 m/s

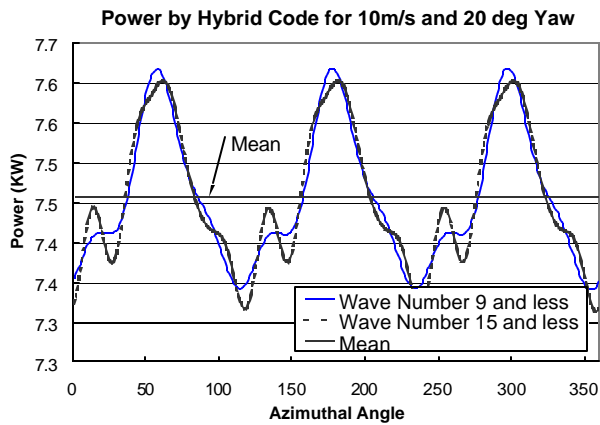


Fig. 7 Hybrid Code Predicted Instantaneous Power Generation for the

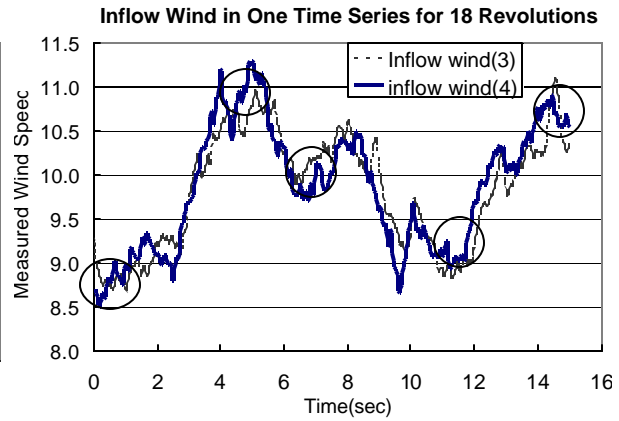


Fig 8. Natural Inflow Wind in an Experimental Time Series for 18

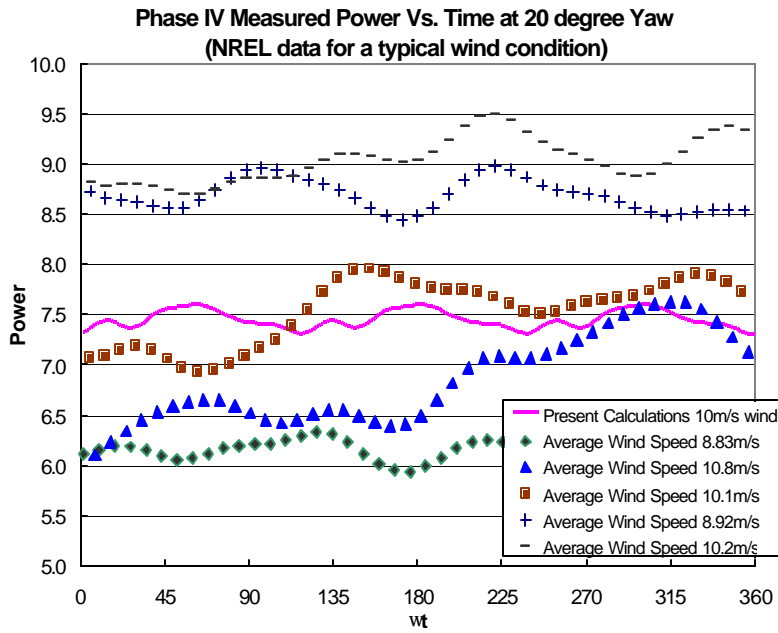


Fig 9 Correlation of Hybrid Yaw Results with Unsteady Measurement

